FUNDAMENTALS & APPLICATIONS

CHEMELECTROCHEM

ANALYSIS & CATALYSIS, BIO & NANO, ENERGY & MORE

Accepted Article

Title: Electrochemical doping as a way to enhance water photooxidation on nanostructured nickel titanate and anatase electrodes

Authors: María Isabel Díez-García, Damián Monllor-Satoca, Victor Vinoth, Sambandam Anandan, and Teresa Lana-Villarreal

To be cited as: *ChemElectroChem* 10.1002/celc.201700039

Link to VoR: http://dx.doi.org/10.1002/celc.201700039

A Journal of

ChemPubSoc Europe

WILEY-VCH

www.chemelectrochem.org

Electrochemical doping as a way to enhance water photooxidation on nanostructured nickel titanate and anatase electrodes

María Isabel Díez-García,[a]† Damián Monllor-Satoca,[a,b]† Victor Vinoth,[c] Sambandam Anandan,[c] and Teresa Lana-Villarreal*[1]

Abstract: A number of metal oxides have been proposed as useful materials for the photoelectrochemical (PEC) production of hydrogen from water. However, up to now, an ideal standalone material has not been found. We have investigated the possible use of nickel titanate ($NiTiO_3$) nanorods as a photoanode. Although these electrodes absorb visible light, they show a modest PEC behavior. Interestingly, the photocurrent for water oxidation undergoes a 20-fold enhancement after an optimized reductive electrochemical pretreatment. Here, the induced doping is studied and compared with the corresponding for anatase nanoporous electrodes. The results reveal the key role of the electrolyte pH as well as the size of the electrode building blocks. The photocurrent promotion upon the electrochemical pretreatment can be ascribed to an enhanced charge transport linked to the ability of proton insertion in the crystal structure.

Introduction

During the last years, an impressive effort has been performed to develop efficient semiconductor electrodes suitable for the photoelectrochemical water splitting, harvesting solar energy. Some authors have focused on the pursuit of new materials,[1,2] particularly ternary oxides, while others have dealt with the upgrade of well-known materials such as titanium dioxide (TiO_2). In this regard, today a number of general strategies are considered suitable to improve the photocatalytic efficiency.[3-5] Namely, we can highlight nanostructuring, sensitization, generation of heterojunctions and doping with heteroatoms. Most of these strategies have been optimized for TiO_2 and subsequently, they have been applied to other metal oxide semiconductors.[6]

Over the last decade, doping TiO_2 with heteroatoms, both metallic and non-metallic (e.g. N, F, C), has been widely studied as it allows to expand the light absorption spectrum into the visible region.[3],[5] Nevertheless, such a modification also triggers a significant enhancement in the number of structural defects, which undesirably promotes charge carrier recombination. In this respect, self-doping with Ti^{3+} species is considered particularly beneficial as it leads to visible light absorption and to an increased conductivity while the density of expected defects is minimized.[7] Consequently, an enhancement in the photoelectrochemical activity has been reported by increasing the content of Ti^{3+} species or in other words, the number of oxygen vacancies. Such a doping procedure is traditionally carried out by chemically reducing TiO_2 at high temperatures in a hydrogen atmosphere.[8,9] Concomitantly, in the last years, several authors have proposed a mild electrochemical reductive pretreatment that can also trigger the generation of Ti^{3+} species (and/or oxygen vacancies[10]) in the structure, promoting the TiO_2 performance.[11] In this case, the accumulation of negative charge is compensated by the insertion/adsorption of cations coming from the electrolyte. Although the induced reduction is partially reversible, it improves the photovoltaic efficiency[12] and leads to a photocurrent increase for water photooxidation.[11] The amended behavior has been ascribed to a more rapid electron transport that promotes electron collection, hindering charge recombination.[10,11] This electrochemical reduction has been successfully applied to different TiO_2 structures including single crystals,[13] polycrystals,[14] compact films,[15] nanoparticles, nanowires and nanotubes[15-17] in acidic and neutral electrolytes. Furthermore, the effect of the cation nature (Li^+ or H^+) present in the electrolyte has also been studied;[16,17] however, to the best of our knowledge, the repercussion of the electrolyte pH remains unexplored.

The electrochemical reductive doping has also been applied to other n-type semiconductors such as WO_3[18,19] and doped and un-doped hematite electrodes,[21] but in the latter case, morphological changes upon 20 minutes of reductive treatment were observed, which could be at least partially responsible for the observed changes.[21] Some authors have proposed that the electrochemical doping could be a general route to enhance the performance of metal oxides.[22] Indeed, an oxidative electrochemical pretreatment has also been revealed as a successful strategy to promote the p-type behavior of electrodes based on $CuFe_2O_4$ and zinc copper indium sulfide (ZCIS).[22,23]

Fueled by a growing interest in new materials that could be advantageous for the photoelectrochemical production of hydrogen, ternary oxides have attracted particular attention. The most common approaches adopted in this pursuit involve a bibliographic/theoretical selection of a ternary oxide absorbing in the visible region with the adequate location of the band edges and the ulterior study of its (photo)electrochemical behavior or a

[a] M.I. Díez-García, Dr. D. Monllor-Satoca, Dr. T. Lana-Villarreal
Departament de Química Física i Institut Universitari d'Electroquímica, Universitat d'Alacant, Apartat 99, E-03080 Alicante, Spain
E-mail: Teresa.Lana@ua.es
[b] Dr. D. Monllor-Satoca
Department of Analytical and Applied Chemistry, IQS School of Engineering, Universitat Ramon Llull, Via Augusta 390, E-08017 Barcelona, Spain
[c] V. Vinoth, Dr. S. Anandan
Nanomaterials and Solar Energy Conversion Lab, Department of Chemistry, National Institute of Technology, Tiruchirappalli 620 015, India
† Both authors contributed equally to this work.

Supporting information for this article is given via a link at the end of the document.

combinatorial approach. In this context, $NiTiO_3$ with a calculated band gap of 2.16 eV has been proposed as a promising candidate.[25] With an ilmenite structure, it has the conduction band and valence band edges that appropriately straddle the H^+/H_2 and O_2/H_2O redox potentials, respectively.[26] This allows to use this material as a photoanode material[25-28] for water splitting although some authors have pointed out its limited (photo)(electro)chemical stability.[26,27]

In this work, we corroborate that the electrochemical reduction reversibly promotes the photoelectrochemical behavior of nanoporous TiO_2 and can be extended to ternary $NiTiO_3$ nanorod electrodes. We demonstrate for the first time, that the phenomenon also occurs in basic media (1 M NaOH), being the enhancement for water photooxidation larger than in acid medium. Furthermore, our results also point to the fact that the nature of this effect does not depend exclusively on the chemical nature of the electrode, but on the size of the building blocks constituting the electrode.

Results and Discussion

$NiTiO_3$ nanorods were prepared as mentioned in the experimental section, adapting a previous method.[30,31] The morphology of the electrodes was characterized by Scanning Electron Microscopy (SEM). Figure 1.A shows a representative image of the top view. It can be easily distinguished randomly stacked nanorods with diameters and lengths in the 1-1.5 μm and 5-6 μm ranges, respectively. These one-dimensional structures are characterized by a rough surface. A more detailed morphological analysis by Transmission Electron Microscopy (TEM) (Figure 1.B) showed that they are constructed by aggregated nanoparticles smaller than 100 nanometers in diameter. On the other hand, the X- Ray Diffraction (XRD) analysis revealed (Figure 1.C) the crystalline nature of the sample. The different crystallographic plane diffractions could be indexed as the rhombohedral ilmenite $NiTiO_3$ structure in agreement with the JCPDS file 33-0960, except for a diffraction peak located at 27.5º which indicates some rutile impurities. The ilmenite structure consists on distorted NiO_6 and TiO_6 octahedra distributed in alternating layers along the c-axis. The relatively strong and narrow diffraction peaks indicate a high crystalline degree. The size of the crystallites oriented in the [104] direction was estimated by using the Scherrer equation:

$$D_{hkl} = \frac{K \cdot \lambda}{B \cdot cos\theta} \qquad (1)$$

where λ is the wavelength of the X-rays, θ is the Bragg angle, *B* is the XRD peak full width at half maximum and K is a numerical factor that considers the crystal shape, being 0.9 for spherical nanoparticles. According to this expression, the $NiTiO_3$ nanoparticles have a diameter of 22 nm in agreement with the TEM analysis. Figure 1.D shows the UV-visible diffuse reflectance spectrum, which reflects the yellow-green color of $NiTiO_3$. Aside from an increasingly growing absorption (i.e. reflectance diminution) at short wavelengths, two apparent absorption features at 450 and 510 nm can be distinguished, in agreement with previous results.[31,32] These particular features can be related to the electronic structure of $NiTiO_3$ in which Ni-3d states are localized over the valence band constituted by O-2p orbitals while the bottom of the conduction band is based on Ti-3d orbitals.[33-34] The bands at 450 nm (2.76 eV) and 510 nm (2.43 eV), indicated by arrows a and b in Figure 4.D, have been related to the Ni-3d orbitals that split up into two sub-bands, allowing charge transfer between these sub-bands and the Ti-3d band located at the bottom of the conduction band. The broad absorption at shorter wavelengths is attributed to the charge transfer between O-2p states at the top of the valence band and Ti-3d states at the bottom of the conduction band.[32] The accompanying Tauc plot (inset in Figure 1.D) for this transition reveals a direct band gap[35] of 3.05 eV. This value agrees well with the photon energy required to develop a photocurrent[34] or a photovoltage[30] with $NiTiO_3$ electrodes.

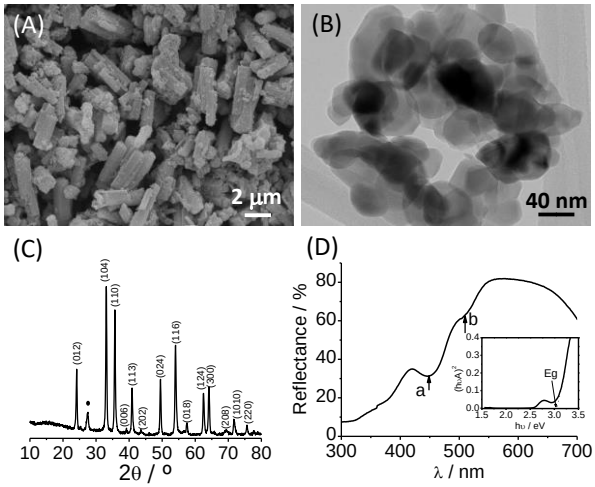

Figure 1. (A) SEM micrograph for an FTO/$NiTiO_3$ electrode; (B) TEM image of $NiTiO_3$ nanoparticles obtained after detaching the $NiTiO_3$ nanorods from the FTO substrate; (C) X-ray diffraction pattern for the as-prepared $NiTiO_3$ powder with the identification of the different crystal orientations (• peak ascribed to rutile impurities) and (D) UV-visible diffuse reflectance spectrum for an $NiTiO_3$ film. The arrows a and b indicate electronic transitions between Ni-3d and Ti-3d. Inset: Determination of the direct optical band gap (the absorbance (A) was estimated from the reflectance measurements using the Kubelka-Munk function).

The electrochemical behavior of $NiTiO_3$ electrodes has been studied in the dark and under transient illumination in N_2-purged 1 M NaOH. As shown in Figure 2, the cyclic voltammogram in the dark is characterized by the presence of capacitive currents at potentials more negative than -0.8 V, as expected for a nanoporous n-type semiconductor. Only a minor faradaic contribution can be observed at potentials more negative than -1.4 V, possibly related to water reduction. By analogy with the behavior observed for nanoporous TiO_2 electrodes,[36] we can ascribe the capacitive currents to the filling of band gap states

and/or states at the bottom of the conduction band. The cyclic voltammogram also exhibits a shoulder at about -0.95 V. Considering the location of the band edges proposed in the literature for $NiTiO_3$,[34,35] it can tentatively be ascribed to the existence of trap states energetically located in the band gap and physically identified as grain boundaries. While the currents appearing at -1.25 V can be tentatively associated with the filling of band gap states just below the conduction band edge or directly conduction band states.

The electron accumulation needs to be accompanied by the adsorption/insertion of cations coming from the electrolyte to preserve the electroneutrality. In view of the aqueous nature of the electrolyte, sodium cation adsorption and/or proton insertion/adsorption can occur. In this regard, although $NiTiO_3$ has been proposed as a material for Li-ion battery anodes,[39] the insertion of Na^+ is unlikely in aqueous media considering the crystalline nature of the nanorods and the large size of solvated Na^+ ions.

Compact $NiTiO_3$ electrodes have been previously studied as photoanodes.[26,28,37,38] At sufficiently positive potentials, anodic photocurrents ascribed to water photooxidation were measured. As shown in Figure 2, the behavior that we observe for the nanoporous electrodes is clearly different. Under illumination, at potentials more positive than -0.63 V, anodic photocurrents are developed, while at potentials more negative than this value, cathodic photocurrents are recorded. Considering the electrolyte composition, and the fact that the material is stable in 1 M NaOH in this potential range, the only possible reactions associated with the photocurrents are water photooxidation (oxygen evolution) and water photoreduction (hydrogen evolution) (See SI, Figure S.1). In other words, $NiTiO_3$ nanorod electrodes behave as photoanodes or photocathodes depending on the applied potential. This behavior agrees well with that expected for a nanoporous semiconductor electrode with a limited charge mobility.[23,39] Under these conditions, the photogenerated charge carrier separation and transport are dominated by the kinetics at the semiconductor-electrolyte interface which depends on the exposed facets[42] and the charge diffusion inside the nanostructure, which is tuned by the substrate potential.

In this work, the possibility of improving the photoelectrochemical behavior of $NiTiO_3$ through an electrochemical reductive pretreatment has been studied and compared with the behavior of nanoporous TiO_2 electrodes based on commercial anatase nanoparticles with polyhedral shapes and with a diameter of about 32 nm (See Figure S.2). These electrodes have already been characterized in 0.1 M $HClO_4$ in a previous work.[11] They showed small photocurrents toward water oxidation and the electrochemical reductive pretreatment only induced a minor enhancement (around 20 % increase).[11] In this study, we have employed nitrogen-purged 1 M NaOH as electrolyte due to the chemical stability restrictions of $NiTiO_3$. This has allowed us to additionally study the electrolyte pH effect on anatase TiO_2 electrodes. It is worth mentioning, that although some authors have pointed out to the possibility that sodium ions from aqueous electrolytes could be

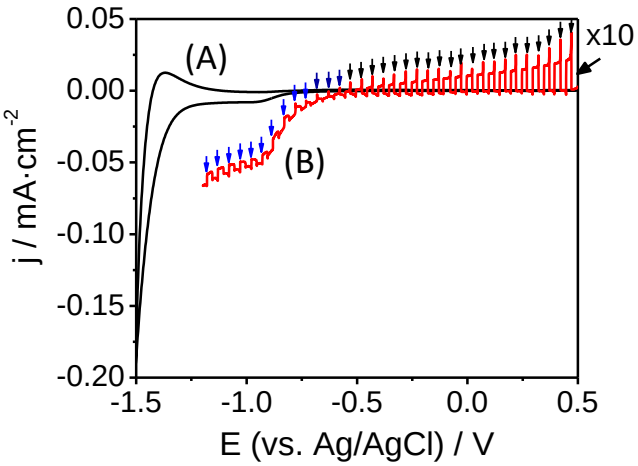

Figure 2. (A) Cyclic voltammogram in the dark for an FTO/$NiTiO_3$ electrode (4.5 µm thickness). Scan rate: 20 mV/s. (B) Linear sweep voltammogram (negative-going scan) under transient illumination. The arrows indicate when the light is turned. Their color indicates if the photocurrent generated is anodic (black) or cathodic (blue). Scan rate: 5 mV/s.

inserted in amorphous TiO_2 electrodes,[40,41] it is unlikely if we consider other reports where a potential below 1 V vs Na^+/Na is established as a requirement for the insertion in anatase nanoparticles.[45] This implies that water reduction is thermodynamically more favored than sodium insertion. Hence, we have not considered the possible insertion of sodium ions as a way to compensate electron accumulation. Obviously, sodium adsorption can occur.

The effect of the electrochemical doping drastically depends on a number of factors, mainly the applied potential and the time, apart from the electrolyte and electrode nature. In order to select the best pretreatment, we have optimized the experimental conditions. First, the potential was amended by applying a step for 4200 s and subsequently, the duration was optimized for the previously selected potential. Figure 3 shows the photocurrent recorded at 0.4 V after performing a potentiostatic step at different potentials for 4200 s for $NiTiO_3$ and TiO_2 nanoporous electrodes. As can be observed, in both cases the photocurrent basically remains unaltered until the pretreatment attains a certain potential value. Once, this potential has been reached, the photocurrent steeply increases and then, it saturates. For longer periods of time, the photoelectrochemical behavior seems to deteriorate. In any case, the photocurrent trend is virtually identical for nanoporous anatase and $NiTiO_3$ electrodes, only the optimized potential is slightly different, being -1.6 V for TiO_2 and -1.5 V for $NiTiO_3$. It should be noted that in both cases, the photocurrent is exclusively promoted when the pretreatment is performed at a potential negative enough to trigger charge accumulation. This can be evinced by the correspondence between the curves of the dependence of the photocurrent on

10.1002/celc.201700039

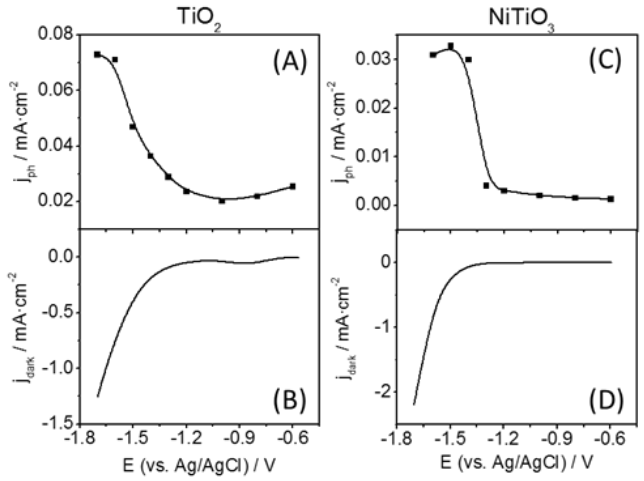

Figure 3. (A, C) Stationary photocurrent at 0.4 V measured after the electrochemical doping at each potential during 4200 s for (A) anatase (3 µm thickness) and (B) $NiTiO_3$ (3.5 µm thickness) electrodes. (B, D) Linear sweep voltammograms (negative-going scan) in the dark for (A) anatase and (B) $NiTiO_3$ electrodes. Scan rate: 20 mV/s.

the pretreatment potential (Figure 3 A and C) and the dark linear scan voltammograms (Figure 3.B and D). This result clearly demonstrates that the photocurrent enhancement after the reductive pretreatment is due to charge accumulation and therefore, to the concomitant insertion of protons coming from the electrolyte. The adsorption of protons/sodium ions is expected to be fully potential reversible (see below) and thus, they are not foreseen to be responsible for the photoactivity enhancement.

Once the optimized potentials were selected, the step duration was refined. Figure 4 shows the dependence of the stationary photocurrent at 0.4 V measured after the electrochemical doping, as a function of the pretreatment time. For both materials, the photocurrent for water photooxidation is clearly promoted with the electrochemical pretreatment in the dark, attaining a maximum enhancement after some time. Note that the time scale employed for both materials is very different. $NiTiO_3$ requires longer times to attain the maximum photocurrent. The charge involved in this process is about 3.5 times larger. However, it cannot be considered a direct measurement of the accumulated electron number, because at -1.5 V (the optimized potential), also water reduction occurs. In

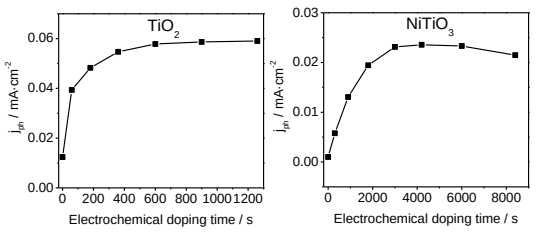

Figure 4. Stationary photocurrent measured at 0.4 V as a function of the electrochemical doping time at -1.6 V for an (A) anatase (3 µm) and at -1.5 V for a (B) $NiTiO_3$ (3 µm) electrodes.

any case, we can consider that the process leading to the photocurrent enhancement is high demanding for $NiTiO_3$, i.e., the required potential is more negative and the optimized time is about one order of magnitude longer than for TiO_2.

As mentioned, the electrochemical doping can be ascribed to the accumulation of electrons with the corresponding insertion of protons. Being the crystal structure of $NiTiO_3$ more open than that of anatase, it should facilitate the diffusion of cations. Nevertheless, charge accumulation occurs more easily in TiO_2. Obviously, apart from the crystal structure, the nanoparticle size and shape can also play a role: the smaller the building blocks constituting the electrode, the shorter the diffusion length of the cations to compensate the electrons and the easier the charge accumulation, i.e. the electrochemical doping. $NiTiO_3$ electrodes are constituted by rods composed of relatively large nanoparticles. The space between these nanoparticles is too small for the electrolyte to permeate, so we can consider the rods as the main building blocks of these electrodes, being the active surface area mainly limited to the rough surface of the nanorods, in agreement with the small capacitive currents observed in Figure 2. To accumulate electrons in the whole structure, the protons should diffuse through such big structures in $NiTiO_3$, while in the case of anatase, the diffusion length is mainly limited to each individual nanoparticle or small aggregates.

On the other hand, the photocurrent is multiplied by a factor of about 5 for anatase and 25 for $NiTiO_3$ electrodes. This is probably linked to the initial larger recombination existing at $NiTiO_3$ electrodes. In this regard, open circuit measurements (see SI, Figure S.3) for $NiTiO_3$ electrodes prior and after the optimized electrochemical doping have revealed, a diminished recombination upon the pretreatment (as shown by the photopotential attained under illumination).

Importantly, in the case of anatase, the enhancement is much larger than in acidic medium, where an enhancement as low as 20 % was detected. This result clearly points to the key role of pH in the electrochemical doping process. Curiously, using the same duration for the electrochemical pretreatment, the enhancement is larger in alkaline medium, where the concentration of protons is smaller. The reason for this behavior is still far from being completely understood, but the fact that the anatase surface is negatively charged in alkaline media could favor the adsorption/insertion of protons. In this regard, there are few publications that have shown that it exists an exponential relation between the charge corresponding to the grain boundary peak and the electrolyte pH[43,44] and these traps have been linked to recombination processes. Hence, in alkaline media, an enhanced recombination is expected, and any modification of the electrode leading to an improvement should be more noticeable.

The comparison of the photoactivity of different electrodic materials is an arduous task, as it is difficult to have electrodes with the same real surface area or absorbing the same number of photons. In our case, the TiO_2 and $NiTiO_3$ electrodes have the same thickness. Although we are aware that we cannot discuss in detail the different factors governing the photoactivity of both materials, from the photocurrents obtained under 100

mW/cm^2 standardized AM 1.5G illumination, it can be concluded that anatase is more efficient for water photooxidation (See SI, Figure S.4). Interestingly, the photocurrent onset and the Mott-Schottky plots revealed a similar apparent flat band potential for both materials (See SI, Figure S.5).

To shed more light on the electrochemical doping effects, the cyclic voltammograms in the dark were measured prior and after the electrochemical reductive pretreatment (Figure 5). Cyclic voltammograms in the dark in the absence of faradaic currents offer a first approach to evaluate the effective density of states. In agreement with the previous results,[11] the pair of peaks ascribed to grain boundaries[48] appearing at -0.8 V (TiO_2) and -0.95 V ($NiTiO_3$) are highly promoted and in the case of anatase, they are clearly displaced toward more positive potential values after the electrochemical pretreatment. It has been proposed that this pretreatment renders a build-up of the space charge layer within the nanoparticle agglomerates in the case of rutile nanoparticles with well-defined surface planes.[11] As the band edges are pinned, such band bending induces the shift of the grain boundary peak toward more positive values. In the case of $NiTiO_3$, the pretreatment also affects the voltammetric behavior in a similar way, although the displacement of the trap peak is not observed so clearly. This can be a consequence of its particular voltammetric shape (they appear as a shoulder), or to the possibility that the band edges of $NiTiO_3$ are unpinned. On the other hand, the fact that the charge involved is enhanced can be considered a consequence of an improved electron transport that facilitates the filling/emptying of the electronic states. In any case, a contribution of an additional hydroxylation of the electrode surface during the electrochemical pretreatment[49] cannot be completely ruled out, particularly in the case of $NiTiO_3$.

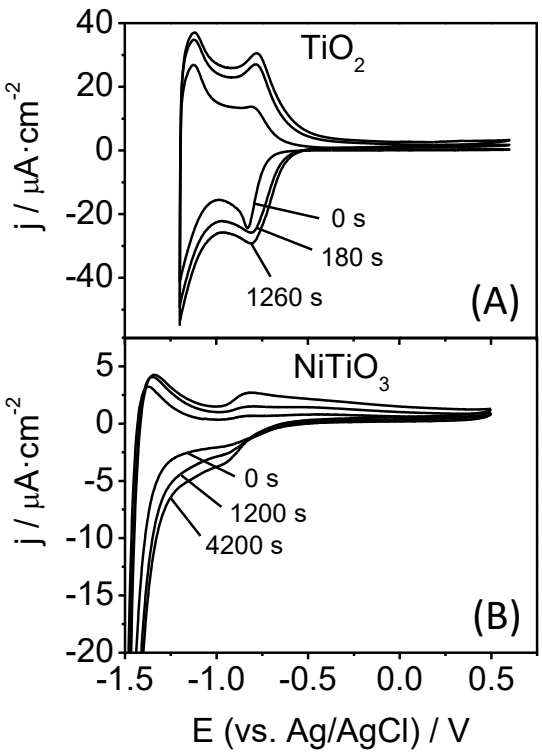

Figure 5. Time evolution of the cyclic voltammograms in the dark with the electrochemical doping time at (A) at -1.6 V for anatase TiO_2 (3.0 μm) and (B) -1.5 V for $NiTiO_3$ (3.5 μm) electrodes. Scan rate: 20 mV/s.

Furthermore, the fact that the different cyclic voltammograms show a symmetric behavior (particularly in the case of anatase), indicates that the electron injection and the corresponding proton/cation uptake processes are reversible in the time scale of the cyclic voltammetry experiment. However, during the electrochemical reductive pretreatment, the electrodes are polarized for longer periods of time and persistent electron accumulation can occur. Note that the charge compensation can exclusively occur through cation adsorption or insertion. Probably, during the cyclic voltammograms, the proton/sodium ions adsorption or the proton intercalation near the surface are the main processes accompanying the electron accumulation. The insertion of protons deeper in the structure is more intricate and it requires applying a sufficiently negative potential for longer periods of time, as during the pretreatment. We can expect that the reduction begins at the outer part of the nanoparticles, particularly at those regions located near the electrode back contact and then, it propagates within shallow and deep internal regions of the nanoparticles. Note that over-insertion can produce water-soluble species,[10] what explains the saturation of the effect, and even a photoactivity worsening. Interestingly, the optimized electrochemical reductive pretreatment does not induce any significant change in the electrode composition, as revealed by XPS spectra (See SI, Figure S.6 and Figure S.7). The question that arises is whether the electrochemical doping effect remains under working conditions (where an anodic current flows) if the electron accumulation and proton uptake are the processes promoting the photoelectrochemical behavior.

Figure 6 shows chronoamperometric measurements for anatase and $NiTiO_3$ nanoporous electrodes. As indicated, the potential program consists in applying a positive bias to measure the photocurrent for water oxidation for the pristine electrodes. After the electrochemical doping, the potential is stepped back to its initial value to measure the photocurrent increase upon the pretreatment. Initially, the reductive doping leads to a 9-fold enhancement for TiO_2 and 30-fold enhancement for $NiTiO_3$ electrodes. After 24 hours, the initial state of the electrode is recovered in the case of anatase, while in the case of $NiTiO_3$ still a 9-fold increase in the photocurrent is recorded. Although the optimized pretreatment is more energetically demanding for $NiTiO_3$ than for TiO_2, the relaxation kinetics for $NiTiO_3$ is also slower. This agrees well with the idea of cation (proton) insertion in the structure during the electrochemical pretreatment, as the slower the proton uptake, the slower the photocurrent multiplication relaxation. The improved photoelectrocatalytic activity toward water oxidation observed upon the optimized reductive pretreatment can be explained by the above

10.1002/celc.201700039

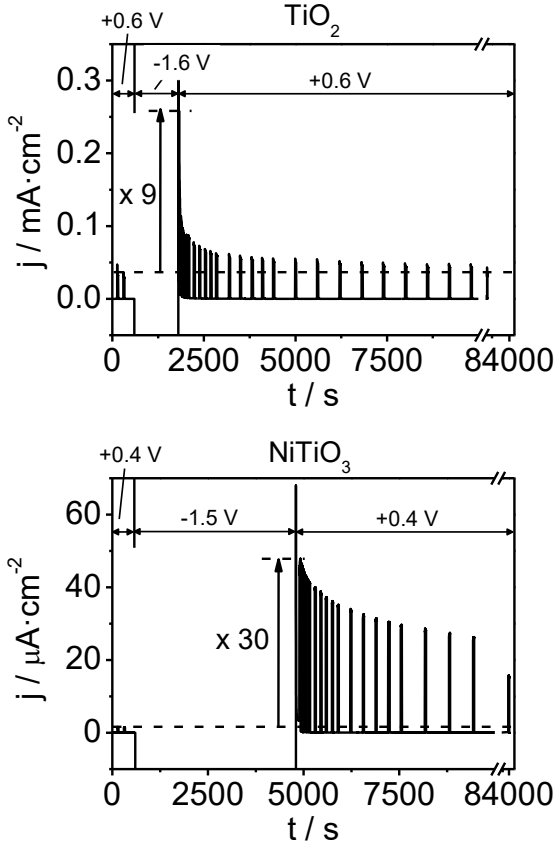

Figure 6. Chronoamperometric measurements under chopped illumination showing the effect of the application of the electrochemical reductive pretreatment on the water photoooxidation current for (A) anatase (3 µm) and (B) $NiTiO_3$ (3 µm) electrodes. The initial photocurrent is indicated by a discontinuous line. The potential program employed in the experiments is indicated in the upper part of each graph.

mentioned electron injection/proton uptake. This process induces (at least temporally) an increase of the majority charge carriers of the electrodes, which favors the electron transport and even build-up of a space charge layer through the nanoparticles aggregates that favor the photogenerated charge carriers separation. In nanoporous n-type semiconductor electrodes, the charge transport is often a limiting factor of the final efficiency because the recombination probability increases as the transport time is longer. In fact, the use of one-dimensional structures has been shown to be a promising strategy to enhance the behavior in many applications.[48,49] Therefore, it is not surprising that an improved electron transport provokes an enhancement of the photocurrent, due to a diminished recombination. In fact, open circuit measurements (see SI, Figure S.3) for $NiTiO_3$ electrodes prior and after the optimized electrochemical doping have revealed not only a diminished recombination, but a smaller electron lifetime (a faster photopotential decay is observed), which is a good indication of a faster electron transport.

Conclusions

$NiTiO_3$ randomly oriented nanorod electrodes exhibiting visible light absorption can be easily prepared. These electrodes can be used as photoanodes for water oxidation, although their efficiency is modest. Their photoelectrochemical behavior can be greatly promoted by an electrochemical reductive pretreatment. Such a pretreatment, once optimized, promotes the electron transport, reducing electron-hole recombination. The photocurrent for oxygen evolution experiences up to a 25-fold enhancement.

To obtain a deeper understanding, the effect of the electrochemical pretreatment is compared with that shown by anatase electrodes based on commercial nanoparticles. The results indicate that the doping process is pH-dependent, being the promotion of the photocurrent higher in alkaline media. Furthermore, the process is also sensitive to the specific electrodic area and consequently to the building block size: the electrochemical doping is facilitated for the smallest. This agrees well with the idea of proton uptake during the reductive pretreatment and the duration of the effect. The results highlight the potential of the optimized reductive electrochemical doping procedure as a general tool to reversibly enhance the activity of nanoporous n-type semiconductor electrodes for water photooxidation.

Experimental Section

Preparation of $NiTiO_3$ nanorods

One-dimensional $NiTiO_3$ nanorods were prepared using a sol-gel route. Namely, 2.48 g of nickel acetate were dissolved in 60 mL of ethylene glycol. Subsequently, 3.4 mL of titanium isopropoxide were added drop-wise under constant stirring at room temperature. The resulting green color suspension was stirred in air for 2 h. After this step, the suspension color turned into light blue, which was indicative that the reaction was completed. The light blue precipitate was recovered by vacuum filtration, washed with ethanol several times and dried under vacuum at 80 °C for 1 h. Finally, the precipitate was calcined at 600 °C for 2 h in air to obtain the desired $NiTiO_3$ nanorods.

Electrode preparation

Electrodes based on $NiTiO_3$ nanorods were fabricated on $F:SnO_2$ – coated glass (FTO, Pilkington TEC15) by the well-known doctor blade method. An aqueous slurry was prepared by grinding 25 mg of the as-prepared $NiTiO_3$ nanorods powder, 7 µL acetylacetone, 7 µL Triton 100X with 125 µL of ultrapure water. Some droplets of this paste were spread over ~1 cm^2 of the substrate, dried at ambient temperature, and annealed at 600 ºC for 1 h in air to sinter the nanorods between them and with the substrate. In a similar way, TiO_2 nanoporous electrodes based on commercial anatase nanoparticles (Alfa Aesar, 99.9%) were also prepared but fired at 450 ºC for 1 hour. The thickness of the resulting films was measured with an Alpha Step D-100 profilometer.

Electrode characterization

A morphological characterization of the as-prepared $NiTiO_3$ powder was carried out by TEM with a JEM-2010 (JEOL) microscope. The electrode morphology was studied by SEM with a JSM-840 (JEOL). The crystal structure was analyzed by XRD with a Seifert JSO-Debyeflex 2002 diffractometer using the Cu Kα line (λ = 1.5406 Å). A Shimadzu UV-2401PC spectrophotometer equipped with an integrating sphere coated with $BaSO_4$ was used to measure UV-visible diffuse reflectance spectra of the $NiTiO_3$ films.

(Photo)electrochemical measurements were performed at room temperature in a three-electrode cell equipped with a fused silica window. All the potentials were measured against and are referred to an Ag/AgCl/KCl (3 M) reference electrode. A platinum wire was used as a counter electrode and an N_2-saturated 1 M NaOH solution as a working electrolyte. Measurements were carried out with a computer-controlled Autolab PGSTAT30 potentiostat. A 1000 W Hg(Xe) lamp (Newport) equipped with a water filter and a cutoff filter (cutoff wavelength of 350 nm), Newport model FSR-KG3) and a 300 W Xe lamp (Thermo Oriel) equipped with a water filter were used as a UV-visible light source to illuminate the $NiTiO_3$ and the TiO_2 electrodes, respectively.

Acknowledgements

We are grateful to the Spanish Ministry of Economy and Competitiveness (MINECO) for financial support through projects PRI-PIBIN-2011-0816 and MAT2012-37676 and MAT2015-71727-R (co-financed with FEDER funds by the European Union). S.A. also thanks DST, New Delhi for the sanction of India–Spain collaborative research grant (DST/INT/Spain/P-37/11 dt.16th Dec 2011). D. M-S. acknowledges MINECO for financial support through project MAT2014-59961-C2-2-R, and the Spanish Ministery of Education and Science for the award of an FPI Fellowship (BES-2004-5194).

Keywords: Nickel titanate • Anatase • Electrochemical doping • Photoelectrochemistry • Water Splitting

[1] F. E. Osterloh, *Chem. Mater.* **2008**, *20*, 35–54.

[2] A. Kubacka, M. Fernández-García, G. Colón, *Chem. Rev.* **2012**, *112*, 1555–1614.

[3] M. Ni, M. K. H. Leung, D. Y. C. Leung, K. Sumathy, *Renew. Sust. Energ. Rev.* **2007**, *11*, 401–425.

[4] M. Pelaez, N. T. Nolan, S. C. Pillai, M. K. Seery, P. Falaras, A. G. Kontos, P. S. M. Dunlop, J. W. J. Hamilton, J. A. Byrne, K. O. Shea, et al., *Appl. Catal. B, Environ.* **2012**, *125*, 331–349.

[5] X. Chen, S. S. Mao, *Chem. Rev.* **2007**, *107*, 2891–2959.

[6] F. E. Osterloh, *Chem. Soc. Rev.* **2013**, *42*, 2294–2320.

[7] F. Zuo, L. Wang, T. Wu, Z. Zhang, D. Borchardt, P. Feng, *J. Am. Chem. Soc.* **2010**, *132*, 11856–11857.

[8] X. Chen, L. Liu, Z. Liu, M. A. Marcus, W. Wang, N. A. Oyler, M. E. Grass, B. Mao, P. Glans, P. Y. Yu, et al., *Sci. Rep.* **2013**, *3*, 1–7.

[9] N. Liu, C. Schneider, D. Freitag, M. Hartmann, U. Venkatesan, J. Müller, E. Spiecker, P. Schmuki, *Nano Lett.* **2014**, *14*, 3309–3313.

[10] Z. Li, Y. Ding, W. Kang, C. Li, D. Lin, X. Wang, Z. Chen, M. Wu, D. Pan, *Electrochim. Acta* **2015**, *161*, 40–47.

[11] T. Berger, T. Lana-Villarreal, D. Monllor-Satoca, R. Gómez, *Electrochem. commun.* **2006**, *8*, 1713–1718.

[12] J. Idígoras, T. Berger, J. A. Anta, *J. Phys. Chem. C* **2013**, *117*, 1561–1570.

[13] H. Pelouchova, P. Janda, J. Weber, L. Kavan, *J. Electroanal. Chem.* **2004**, *566*, 73–83.

[14] S. E. Lindquist, A. Lindgren, C. Leygraf, *Sol. Energy Mater.* **1987**, *15*, 367–382.

[15] M. Zukalova, M. Bousa, Z. Bastl, I. Jirka, L. Kavan, *J. Phys. Chem. C* **2014**, *118*, 25970–25977.

[16] C. Xu, Y. Song, L. Lu, C. Cheng, D. Liu, X. Fang, X. Chen, X. Zhu, D. Li, *Nanoscale Res. Lett.* **2013**, *8*, 391.

[17] L. Tsui, M. Saito, T. Homma, G. Zangari, *J. Mater. Chem. A* **2015**, *3*, 360–367.

[18] B. H. Meekins, P. V Kamat, *ACS Nano* **2009**, *3*, 3437–3446.

[19] S. J. Calero, P. Ortiz, A. F. Oñate, M. T. Cortés, *Int. J. Hydrogen Energy* **2016**, *41*, 4922–4930.

[20] J. Zhao, E. Olide, F. E. Osterloh, *J. Electrochem. Soc.* **2014**, *162*, H65–H71.

[21] P. Shangguan, S. Tong, H. Li, W. Leng, *RSC Adv.* **2013**, *3*, 10163.

[22] G. Wang, Y. Yang, Y. Ling, H. Wang, X. Lu, Y.-C. Pu, J. Z. Zhang, Y. Tong, Y. Li, *J. Mater. Chem. A* **2016**, *4*, 2849–2855.

[23] N. Guijarro, T. Lana-Villarreal, R. Gómez, *Chem. Commun. (Camb).* **2012**, *48*, 7681–3.

[24] M. . Díez-García, T. Lana-Villarreal, R. Gómez, *ChemSusChem* **2016**, *9*, 1504–1512.

[25] C. Xin, Y. Wang, Y. Sui, Y. Wang, X. Wang, K. Zhao, Z. Liu, B. Li, X. Liu, *J. Alloys Compd.* **2014**, *613*, 401–406.

[26] P. Salvador, C. Gutierrez, J. B. Goodenough, *J. Appl. Phys.* **1982**, 7003.

[27] C. Gutierrez, P. Salvador, J. B. Goodenough, *J. Electroanal. Chem. Interfacial Electrochem.* **1982**, *134*, 325–334.

[28] P. H. M. de Korte, G. Blasse, *J. Solid State Chem.* **1982**, *44*, 150–155.

[29] A. A. Tahir, M. Mazhar, M. Hamid, K. G. U. Wijayantha, K. C. Molloy, *Dalton Trans.* **2009**, *2*, 3674–80.

[30] Y. Qu, W. Zhou, Z. Ren, S. Du, X. Meng, G. Tian, K. Pan, G. Wang, H. Fu, *J. Mater. Chem.* **2012**, *22*, 16471.

[31] S. Anandan, T. Lana-Villarreal, J. J. Wu, *Ind. Eng. Chem. Res.* **2015**, *54*, 2983–2990.

[32] Y. J. Lin, Y. H. Chang, W. D. Yang, B. S. Tsai, *J. Non. Cryst. Solids* **2006**, *352*, 789–794.

[33] J. B. Bellam, M. A. Ruiz-Preciado, M. Edely, J. Szade, A. Jouanneaux, A. H. Kassiba, *RSC Adv.* **2015**, *5*, 10551–10559.

[34] P. Salvador, C. Gutierrez, J. B. Goodenough, *J. Appl. Phys.* **1982**, *53*, 7003–7013.

[35] M. A. R. Preciado, A. Kassiba, *RSC Adv.* **2015**, *5*, 17396–17404.

[36] T. Berger, D. Monllor-Satoca, M. Jankulovska, T. Lana-Villarreal, R. Gómez, *ChemPhysChem* **2012**, *13*, 2824–2875.

[37] Y. Zhang, J. Gu, M. Murugananthan, Y. Zhang, *J. Alloys Compd.* **2015**, *630*, 110–116.

[38] X. Yong, M. A. A. Schoonen, *Am. Mineral.* **2000**, *85*, 543–556.

[39] V. D. Nithya, R. K. Selvan, K. Karthikeyan, Y. S. Lee, *J. Nanosci. Nanotechnol.* **2015**, *15*, 694–702.

[40] P. H. M. de Korte, G. Blasse, *J. Solid State Chem.* **1982**, *44*, 150–155.

[41] A. K. Díaz-García, M. I. Díez-García, T. Lana-Villarreal, R. Gómez, *Electrochim. Acta* **2016**, *219*, 453–462.

[42] K. M. Macounova, M. Klusáčková, R. Nebel, M. Zukalova, M. Klementova, I. E. Castelli, M. D. Spo, J. Rossmeisl, L. Kavan, P. Krtil, *J. Phys. Chem. C* **2017**, acs.jpcc.6b09289.

[43] F. C. El Moursli, Z. Edfouf, F. Hajji, K. Nabih, K. Nouneh, M. Abdlefdil, *Renew. Sustain. Energy Conf. (IRSEC), 2014 Int.* **2014**, 2–6.

[44] M. Cabello, G. F. Ortiz, M. C. López, R. Alcántara, J. R. González, J. L. Tirado, R. Stoyanova, E. Zhecheva, *J. Alloys Compd.* **2015**, *646*, 816–826.

[45] Y. Xu, E. M. Lotfabad, H. Wang, B. Farbod, Z. Xu, A. Kohandehghan, D. Mitlin, *Chem. Commun.* **2013**, *49*, 8973–8975.

[46] H. Wang, J. He, G. Boschloo, H. Lindström, A. Hagfeldt, S.-E. Lindquist, *J. Phys. Chem. B* **2001**, *105*, 2529–2533.

[47] M. Jankulovska, T. Berger, S. S. Wong, R. Gómez, T. Lana-Villarreal, *ChemPhysChem* **2012**, *13*, 3008–3017.

[48] M. Jankulovska, T. Berger, S. S. Wong, R. Gómez, T. Lana-Villarreal, *ChemPhysChem* **2012**, *13*, 3008–3017.

[49] X. Lu, G. Wang, T. Zhai, M. Yu, J. Gan, Y. Tong, Y. Li, *Nano Lett* **2012**, *12*, 1690–1696.

[50] M. Ge, C. Cao, J. Huang, S. Li, Z. Chen, K.-Q. ZHANG, S. S. Al-deyab, Y. Lai, *J. Mater. Chem. A* **2016**, *4*, 6772–6801.

[51] J. Tian, Z. Zhao, A. Kumar, R. I. Boughton, H. Liu, *Chem. Soc. Rev.* **2014**, *43*, 6920–6937.

10.1002/celc.201700039

Entry for the Table of Contents (Please choose one layout)

ARTICLE

Improving the photoinduced OER: A controlled electrochemical pretreatment provokes a reductive doping for both, nanoporous $NiTiO_3$ and anatase electrodes. Such a process depends on the electrode morphology and electrolyte pH. It improves the charge transport increasing the photocatalytic water oxidation activity.

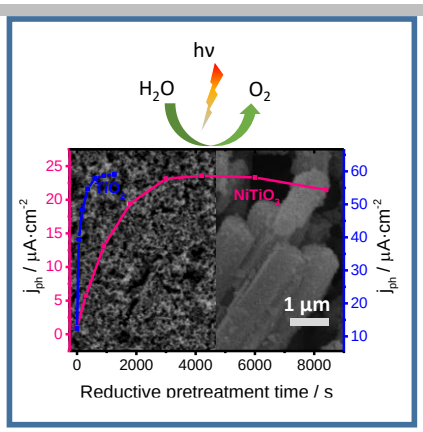

*M.I. Díez-García, D. Monllor-Satoca, V. Vinoth, S. Anandan, T. Lana-Villarreal**

Page No. – Page No.

Electrochemical doping as a way to enhance water photooxidation on nanostructured nickel titanate and anatase electrodes